metals

MDPI

Article

Spatial Distribution of Wettability in Aluminum Surfaces Treated with an Atmospheric-Pressure Remote-Plasma

José Muñoz *, Rocío Rincón and María Dolores Calzada

Laboratorio de Innovación en Plasmas, Edificio Einstein (C2), Campus de Rabanales, Universidad de Córdoba, 14071 Córdoba, Spain

* Correspondence: jmespadero@uco.es; Tel.: +34-957-218-627

Received: 14 August 2019; Accepted: 26 August 2019; Published: 27 August 2019

Abstract: The use of atmospheric-pressure remote plasmas (postdischarge) sustained in argon and argon–nitrogen for the treatment of aluminum surfaces has been studied to better understand the underlying mechanisms responsible for cleaning and activating the surfaces. The effect of the gas composition, treatment distance, and speed on the hydrophilicity of commercial aluminum samples has been studied using the sessile drop method to build spatial profiles of the treated zones. In the case of argon–nitrogen postdischarges, neither the distance to the plasma end ($2 < z < 6$ cm) nor the treatment speed ($2500 < v < 7500$ µm/s) had a significant impact in the spot radius of the treatment, remaining approximately constant around 6–7 mm. This result seems to indicate that the postdischarge experiments a little expansion at the exit of the tube in which the discharge was created but its action can be considered highly-directional. This fact is essential for the possible industrial implementation of the procedure described in this research. These results have been analyzed together with the composition of active species in the postdischarge by using optical emission spectroscopy, revealing that long lived nitrogen species are required to significantly increase the wettability of the aluminum surfaces.

Keywords: aluminum; surface; plasma; nitrogen; postdischarge; atmospheric pressure; wettability

1. Introduction

Among the different materials used in the industry, metals and their alloys stand out due to their outstanding properties such as thermal and electric conductivity, malleability or ductility which make them of special interest to be utilized in sectors like electronics, food packaging, automotive, aeronautics, or construction. Aluminum is one of the most used metals, and from the environmental point of view, it is 100% recyclable without the loss of any of its properties, thus guaranteeing the development of sustainable technologies on the long term. However, this strategic material is often exposed to harsh environments that provoke fast oxidation and/or corrosion of its surface. For example, in the development of lithium-ion batteries, it is common to use aluminum for the manufacture of the current collector, which is exposed to the pitting corrosion of the electrolytes of the battery, especially during long work cycles, like those required for their use in electric and/or hybrid cars. This deterioration can cause an increase in the impedance and self-discharge of the battery, as well as loss of its energy storage capability [1]. Similarly, aluminum surfaces can be easily damaged by corrosion due to chlorine ions, which is of great importance during the continue exposure to environmental agents of aluminum components in construction, naval, and aerospace industries [2].

Therefore, the development of a correct protection on aluminum surfaces, e.g., by depositing a protective film on the metallic material, becomes crucial to the achievement of significant advances

in the demanding construction industry or the implementation of energy storage. Nevertheless, the inclusion of a protective film on aluminum surfaces requires an effective adhesion between them. Among other methodologies, plasma technology has demonstrated its capability to improve the adherence of different material surfaces by inducing changes on their surface energy and thus on their wettability behavior [3–5]. The role of the plasma in this process can be understood as an initial conditioning of the surface by two different approaches. On the one hand, energetic plasma species can remove impurities from the metal surface thus cleaning the surface and, on the other hand, during the plasma process, new surface functional groups, e.g., hydroxyl groups, can be inserted or deposited, thus activating the surface.

Dielectric Barrier Discharges (DBDs) have been used for the activation of surfaces of steel [6], chromium [7], and aluminum [8–10] because their geometry is more suitable for treating flat surfaces in continuous mode. However, some studies have explored the possibility of using other plasma sources for this purpose, such as radiofrequency or microwave plasmas [11–14], more suitable for the treatment of small and/or irregular surfaces.

In a previous investigation [14], the remote plasma (postdischarge) of argon and argon–nitrogen microwave plasmas was used for cleaning and activating the surface of commercial aluminum samples. The action of the postdischarge on the considered surfaces provoked a significant increase of the hydrophilicity and surface energy from 37 to values ranging from 69 (Ar postdischarge) to 77 mJ/m^2 (Ar-N_2 postdischarge)—values comparable and even larger than those required by the industrial processing standards for the deposition and adhesion of films on the metal surfaces. Besides, the effectiveness of the postdicharge treatment for distances up to 5 cm was tested; this distance being larger than those typically allowed by Dielectric Barrier Discharge (DBD) by an order of magnitude. In addition, the use of microwave plasmas allows for treating non-planar geometries, an advantage with respect to DBD discharges, which are limited to the treatment of flat surfaces.

The present work is a continuation of our previous investigation on the action of the microwave-plasma postdischarge to clean and activate aluminum metal surfaces [14]. The current research is devoted to analyzing the spatial resolution of the treatment carried out by the Ar-N_2 postdischarge as well as the surface mechanism during the postdischarge action on the aluminum surface.

2. Experimental and Methods

Figure 1a shows a diagram of the experimental setup used for creating and treating aluminum samples; a picture of the plasma and postdischarge can be observed in Figure 1b.

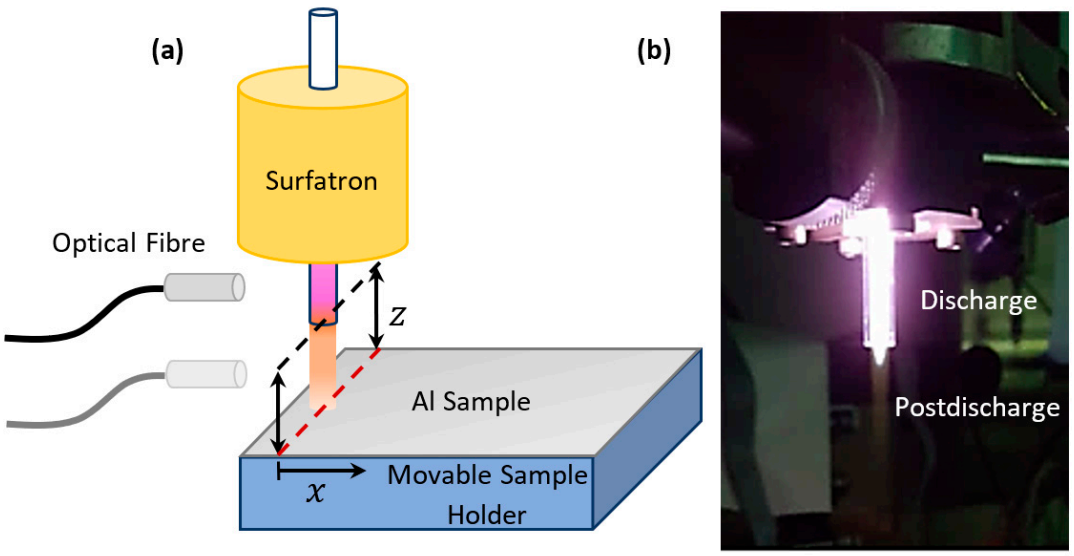

Figure 1. Experiment setup (**a**) and detail of an Ar-N_2 discharge and (**b**) postdischarge.

A Sairem GMP 03 k/SM microwave (2.45 GHz) generator (Sairem Ibérica S.L., Barcelona, Spain) supplied power of 150 W in continuous mode to create and maintain the surface-wave plasmas and a surfatron [15] was used as energy coupling device. Surface-wave discharges were created in quartz tubes of 2 and 3 mm of inner and outer radius, respectively, opened to the atmosphere at one of its ends. This tube extends 3 cm from the launching gap of the surfatron and the postdischarge expanded out the tube (Figure 1a). The adjustable capacity coupler of the surfatron and a triple coaxial stub allowed microwave power to be coupled to the discharge with a maximum of 5% reflected power.

Gas mixtures of Ar-N_2 with a N_2 maximum content of 1% were obtained from high-purity (>99.999%, Abello Linde S.A., Seville, Spain) Ar and N_2 gases, whose flows were controlled by mass flow controllers (HI-TEC, Bronkhorst, Iberfluid Instruments S.A., Barcelona, Spain). The total gas flow used in all experiments was kept at 1 slm (standard liter per minute).

When nitrogen takes part in the plasma gas mixture, two changes take place in the morphology of the plasma. Firstly, the discharge expands radially due to the higher thermal conductivity of the mixed plasma gas relative to that in pure Ar gas [16]. Due to the high temperatures and the presence of active species, this expansion can erode the tube containing the plasma and incorporate the ablated material to the discharge, thus the maximum nitrogen amount considered in the current work was chosen to ensure the integrity of quartz tube containing the discharge [17] and avoiding the contamination of plasma gas. Secondly, the addition to a pure Ar discharge, even in small amounts, leads to a noticeable reduction of plasma column length and the appearance of a postdischarge containing active species and very few or no charged particles, where neutral excited species with long lifetimes control its internal kinetics [18,19]. The experimental conditions considered in the current work ensured the obtention of a postdischarge long enough to act on the surface of the aluminum samples. Depending on the pressure conditions under which the plasma is generated, the nitrogen proportion in the Ar-N_2 mixture as well as the total plasma gas flow, two distinct regions can be observed in the postdischarge: (a) The early postdischarge (EAP), named pink afterglow as a results of the First Negative System (FNS) emission of N_2^+ in the 325–590 nm range, and (b) the late postdischarge (LAP) characterized by an orange color because of the emission of the First Positive System (FPS) of N_2 in the 500–1000 nm interval. In Figure 1b, a photograph corresponding to Ar-N_2 (1% N_2) used in the current investigation allows us to observe the plasma and the postdischarge; this last one expands in the air which leads to a reduction of its length in comparison to the postdischarges generated inside the same discharge tube in which the plasma is created [20,21]. This shortening could be due to the deexcitation of the excited neutral species of N_2, coming from the plasma, with the air surrounding the postdischarge.

The species generated into the plasma and the postdischarge were identified from the analysis of the radiation collected by an optical fibre of 1000 μm in diameter placed perpendicular to the tube axis (Figure 1a) and driven to the entrance slit of a monochromator (FHR-640, Jobin–Yvon Horiba, M.T. Brandao S.L., Madrid, Spain) type Czerny–Turner equipped with 2400 lines/mm holographic grating (200–750 nm range) and equipped with a Charge-Coupled Device (CCD) camera (Symphony, Jobin–Yvon Horiba, M.T. Brandao S.L., Madrid, Spain) as detector.

The aluminum samples (2.5 × 2.5 cm) were obtained from commercial aluminum coil whose surface composition was already analyzed in a previous work [14], mainly consisting of Al, O, C, and F. These samples were prepared following the procedure described in our previous work [14]: after cutting, samples were cleaned in an ultrasonic bath with acetone for 5 min and later they were dried in contact with air. Later, the samples were rinsed with ethanol and dried. This procedure is similar to that employed by other authors [7,12,13] and serves only to the purpose of removing the solid impurities on the material surface before the postdischarge treatment.

In order to determine the effective surface area treated by the postdischarge (spatial resolution), the wettability of the aluminum surfaces under the different conditions considered in the current study was measured from the water contact angle (WCA) of drops placed on the sample surfaces. For the measurement of the contact angle, the sessile drop method reported in [22] was used. Water drops of 5 μL (micro-liter) were deposited on aluminum surface after the treatment using a micropipette

and pictures right after the deposition were taken by a Casio EXFH20 digital camera (Casio, Tokyo, Japan) with a focal distance of 5 mm and exposure time of 1/6 s (Figure 2). The values of the contact angle were obtained from three samples treated under the same experimental conditions and taken at different positions away from the tube axis (x = 0 mm), i.e., treatment axis (Figure 1a).

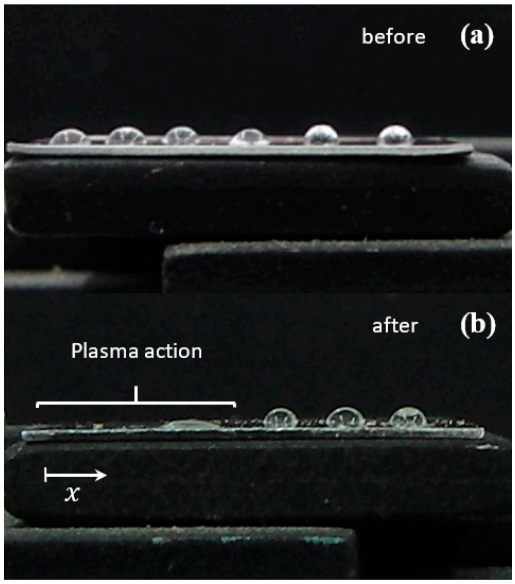

Figure 2. Photographs of water drops deposited in an aluminum sample before (**a**) and after the treatment (**b**) (1% N_2 in Ar-N_2, 150 W).

For their exposition to the postdischarge, the samples were placed on a two-dimensional displacement system formed by two linear actuators (T-LSM50B, Zaber Technologies Inc., Vancouver, BC, Canada); the movement of these actuators was controlled using a script executed in a Zaber console system. In Figure 1a, a red dash-line shows the movement of the platform on which the samples are placed. In order to obtain information about the spatial distribution of the proposed treatment, different experiments were carried out. In this way, the samples were placed at different distances (z) measured from the end of the discharge tube (Figure 1a), which matched the end of the discharge and, therefore, the beginning of the postdischarge. Due to the dimensions considered in this research, aluminum samples were only treated by the late postdischarge (see Figure 1b). Besides, the influence of the exposition time of the samples to the postdischarge was also studied as a function of the different speeds of the sample holder (v). For the purpose of ensuring the reproducibility of the treatment, different sets of experiments were carried out. In this sense, the resulting WCA profiles shown in Section 3.3 were built from the superposition of the measurements along the x direction, perpendicular to the treatment (Figure 1a), carried out in three different samples treated using the same conditions.

3. Results and Discussion

3.1. Active Species in the Discharge

The existence of the postdischarge area shows that Ar-N_2 discharges can be utilized to generate active species that can be used for remote surface treatment. Thus, a brief study of Ar-N_2 discharge by means of its emitted spectrum has been conducted to understand the formation of active species in the postdischarge.

Typical spectrum emitted by an Ar-N_2 (1%) discharge is shown in Figure 3, together with the spectrum emitted by a pure Ar discharge for comparison purposes. In pure Ar (Figure 3a), the spectrum is dominated by emissions belonging to the argon atomic system. Besides, only molecular bands corresponding to excited molecular radicals such as OH $\left(A^2\Sigma^+ \rightarrow X^2\Pi\right)$ and NH $\left(A^3\Pi \rightarrow X^3\Sigma^-\right)$ are

observed. These radicals reveal the presence of water and nitrogen as impurities contained in the plasma gas since the discharge is contained in the quartz tube without being in contact with air. When N_2 is present in the plasma gas even in concentrations as low as 1% (Figure 3b), the spectral lines corresponding to 5p and upper levels of argon atomic system practically disappear and only few lines for 4p levels can be observed, and the Ar-N_2 spectrum is dominated by molecular bands from the radiation emitted by the nitrogen excited molecules and molecular ions (N_2^+).

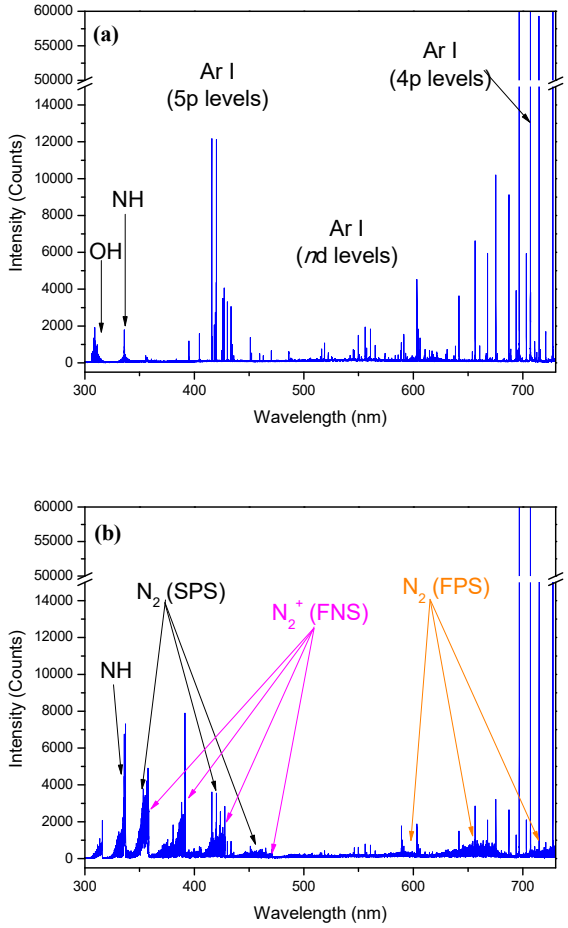

Figure 3. Optical emission spectra of a pure Ar (**a**) and an Ar-N_2 (1% N_2) (**b**) plasma.

In Figure 4, the main energy levels of Ar, N_2 molecule, and N_2^+ molecular ion are depicted; it can be seen that the mestastable levels of nitrogen, represented by $N_2\left(A^3\Sigma_u^+\right)$, have an energy equal to 6.17 eV which is lower than the mestastable level for Ar atom (11.5 eV). In plasmas generated at atmospheric pressure, the excitation/ionization processes are controlled by collisions with electrons, being carried out in steps, being the first excited levels (metastables) the departure levels for these processes [23–26]. This fact, together with the difference between the energies of metastable levels for Ar and N_2, induces a quick increase on the intensities of N_2 molecular and N_2^+ bands and significant changes in the emission of excited Ar atoms (Figure 3) when nitrogen is present. These differences are due to the competition of Ar metastable states and N_2 molecules at ground state for the plasma electrons of low energies (4–7 eV) (Figure 4), contributing to break the stepwise excitation chain of Ar atoms, which is reflected in the strong decrease in the radiation emission coming from the 5p and upper levels belonging to the Ar atomic system. This behavior is opposite to that found in Ar-He and Ar-Ne discharges, where the spectra are dominated by emissions of excited Ar atoms since the excitation of their metastable states requires collisions with electrons with energies higher than for Ar (19.8 and 16.6 eV for He and Ne, respectively) [27,28].

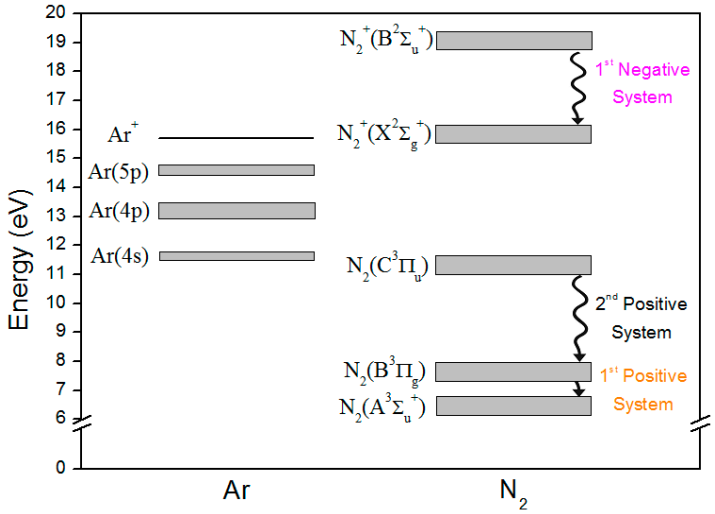

Figure 4. Main energy levels for the Ar atom and the N_2 molecule.

However, besides inelastic collisions with electrons, the formation of nitrogen excited species leading to the appearance of molecular bands in the spectra recorded for Ar-N_2 plasmas is also affected by processes involving heavy particles. Penning excitation (1), is the most probable for the excitation of nitrogen molecules up to $N_2\left(C^3\Pi_u\right)$ state [29]. This reaction is favored by the nearly resonant energies for these species; that is, 11.50 eV for Ar metastable atoms and 11.03 eV for $N_2\left(C^3\Pi_u\right)$ nitrogen excited molecules (Figure 4). From this level, spontaneous emission reactions (2) and (3), can also contribute to the formation of nitrogen molecules to excited states $N_2\left(B^3\Pi_g\right)$ and $N_2\left(A^3\Sigma_u^+\right)$, and the emission of the SPS and FPS, respectively.

$$Ar^m + N_2\left(X^1\Sigma_g^+\right) \rightarrow N_2\left(C^3\Pi_u\right) + Ar^0 \quad (1)$$

$$N_2\left(C^3\Pi_u\right) \rightarrow N_2\left(B^3\Pi_g\right) + h\nu(SPS) \quad (2)$$

$$N_2\left(B^3\Pi_g\right) \rightarrow N_2\left(A^3\Sigma_u^+\right) + h\nu(FPS) \quad (3)$$

Nitrogen molecular ions (N_2^+) are mostly created by charge transfer reactions (4) due to the resonance in energy of the particles taking part in this reaction [30], 15.6 eV for $N_2^+\left(X^2\Sigma_g^+\right)$ and 15.8 eV for Ar^+.

$$Ar^+ + N_2\left(X^1\Sigma_g^+\right) \rightarrow Ar^0 + N_2^+\left(X^2\Sigma_g^+\right) \quad (4)$$

The excited $N_2^+\left(B^2\Sigma_u^+\right)$, whose emission gives place to the first negative system (5) can be formed from the fundamental level of the molecular ion through inelastic collisions with electrons (6), with other nitrogen excited molecules ($N_2\left(A^3\Sigma_u^+\right)$, $N_2\left(B^3\Pi_g\right)$ and $N_2\left(C^3\Pi_u\right)$) taking part in the creation of fundamental level of ion molecular as intermediate steps.

$$N_2^+\left(B^2\Sigma_u^+\right) \rightarrow N_2^+\left(X^2\Sigma_g^+\right) + h\nu(FNS) \quad (5)$$

$$N_2^+\left(X^2\Sigma_g^+\right) + e^- \rightarrow N_2^+\left(B^2\Sigma_u^+\right) + e^- \quad (6)$$

Finally, formation of nitrogen atoms can be obtained from electron impact dissociation of N_2 molecules at ground state (7) or through processes of dissociative recombination of molecular ions (8) [31].

$$N_2\left(X^1\Sigma_g^+\right) + e^- \rightarrow N + N + e^- \quad (7)$$

$$N_2^+\left(X^2\Sigma_g^+\right) + e^- \rightarrow N + N \quad (8)$$

The presence of nitrogen atoms in the discharge is supported by the emission of the band originated by NH $\left(A^3\Pi\right)$ (Figure 3b), being NH formed by recombination of free nitrogen atoms and hydrogen in the discharge in the presence of a third body (9) [32]. In the case of pure Ar plasma (Figure 3a), the presence of NH bands in the spectrum is due to the nitrogen and hydrogen atoms present in the plasma as impurities.

$$N + H + Ar^0 \rightarrow NH\left(A^3\Pi\right) + Ar^0 \quad (9)$$

3.2. Active Species in the Postdischarge

In surface-wave plasmas, the discharge ends at the point where the wave sustaining the plasma ceases its propagation. Excited particles with long lifetimes, created in the discharge and draught downstream by the gas flow, can still exist outside of the discharge, giving place to the postdischarge. However, since no external power is supplied to the postdischarge, the existence of particles capable of interacting with the samples exposed to them depends entirely on the energy of these long-lived particles and their kinetics. Figure 5 shows the spectra corresponding to the radiation emitted by the postdischarge taken at different distances measured from the end of the discharge tube (plasma end). At z = 0.5 cm, closer the plasma end, OH, NH, N_2, and $N_2{}^+$ molecular transitions (Figure 5a) together with the emissions from the ArI atomic system (Figure 5) can be observed. As we move along the postdischarge, all signals decrease, thus implying a decrease in the concentration of active species.

In particular, the OH band signal can be appreciated at 0.5 cm from the end of the discharge, but it disappears completely at a distance of 3 cm. This fact suggests that no new OH radicals are generated in the postdischarge and mission of the NH band in the postdischarge points out the presence of nitrogen atoms in this region. A decrease of the intensity of this band is related to the reduction of the numthus, its presence is due to transport of this specie by the gas flow from the discharge but not to the interaction with the air surrounding the postdischarge. According to the formation pathway of NH through Equation (9), the eber of N atoms while moving further the end of the discharge. Indeed, from Figure 5a, the presence of N atoms is demonstrated at postdischarge positions of $z = 3$ cm due to the emission of NH band.

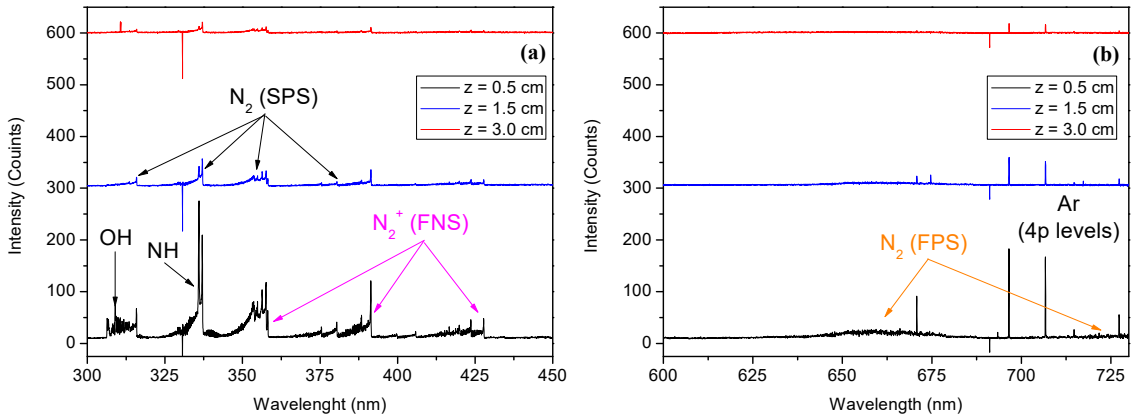

Figure 5. Optical emission spectra of the postdischarge at different axial positions away from the end of the discharge in the (**a**) 300–450 nm and (**b**) 600–730 nm spectral ranges.

The Second Positive System (SPS), whose signal is due to the existence of $N_2\left(C^3\Pi_u\right)$ excited molecules could either be generated by Penning excitation (1) with Ar metastable atoms or by nitrogen metastable pooling (10). Both formation channels are possible since the existence of both Ar metastable atoms and nitrogen $N_2\left(A^3\Sigma_u^+\right)$ metastable molecules in the postdischarge region is demonstrated by the emission of Ar lines and the FPS, respectively.

$$N_2\left(A^3\Sigma_u^+\right) + N_2\left(A^3\Sigma_u^+\right) \rightarrow N_2\left(B^3\Pi_g, C^3\Pi_u\right) + N_2\left(X^1\Sigma_g^+\right) \quad (10)$$

The existence of $N_2\left(B^3\Pi_g\right)$ excited molecules is linked, besides metastable pooling, to the three-body recombination for the nitrogen atoms (11)

$$N + N + Ar^0 \rightarrow N_2\left(B^3\Pi_g\right) + Ar^0 \quad (11)$$

and followed by deexcitation by reaction (3) gives place to the FPS, whose presence indicates the existence of metastable $N_2\left(A^3\Sigma_u^+\right)$ molecules in the postdischarge.

Finally, given that no additional energy is supplied to the postdischarge, very few electrons can be created and most of the electrons coming from the discharge are readily lost by recombination. However, the emission of the FNS of the nitrogen molecular ion can still be detected at $z = 3$ cm.

3.3. Spatial Distribution of the Plasma Action on the Surface of Aluminum Samples

Changes in the WCA measured following the procedure described in Section 2 can provide information about the wettability modifications suffered by the material exposed to the postdischarge. As it has been previously described, treatment profiles were built from the WCAs measured for three different samples which have been plotted with different colors in the following figures (Figures 6, 8 and 9). The resulting profiles were fit to a simple sigmoid function (12)

$$WCA = WCA_{min} + \frac{WCA_{max} - WCA_{min}}{1 - e^{\frac{x - x_0}{dx}}} \quad (12)$$

being WCA_{min} and WCA_{max} the minimum and maximum values of the contact angle, respectively, x_0 the inflection point of the sigmoid function, which can be taken as a measurement of the radius of the treatment spot. Finally, dx is a parameter related to the width of the transition zone between WCA_{min} and WCA_{max}, which in our case was fixed to 0.5 mm for all the profiles as it provided the best fitting results.

In Figure 6, the WCA profile obtained at different positions away from the treated zone for aluminum samples treated with the postdischarges of an Ar and A-N_2 (1%) plasmas appear depicted. For these experiments, samples were located at $z = 4$ cm away from the end of the discharge tube and the displacement speed was maintained constant at 7500 µm/s. The similarity of the profiles obtained for different samples is a prove of the reproducibility of the treatment. The resulting dispersion in WCA values can be explained since all the samples were obtained from commercial aluminum, which can contain imperfections resulting from machining affecting the WCA measurement. To illustrate these imperfections, microscopic images from the samples were taken using a JEOL (Tokyo, Japan) JSM 7800 Prime scanning electron microscope (SEM) (Figure 7). There, striped marks resulting from machining as well as other imperfections are noticed both in the untreated and treated samples. No significant difference in the morphology nor smoothing of the surface can be observed for the case of the treated samples.

From Figure 6, a significant change in the WCA is observed when nitrogen is present in the postdischarge, as compared to the case of the pure Ar postdischarge. In this way, exposing the surface to the postdischarge of a plasma containing 1% N_2 results in an improvement of the wettability properties of the aluminum surfaces showing a decrease of WCA_{min} from 80° to 40°. Studies carried out at atmospheric pressure have suggest that the light emitted by the discharge, containing high-energy photons, might play some role in breaking organic bonds at the surface of polymeric materials [33]. However, our results points to an important role of the nitrogen species in the modification of the wettability of the surfaces. Indeed, similar studies performed at reduced pressures have suggested that nitrogen atoms can play a significant role in the cleaning process of iron foils, where aliphatic carbon atoms existing in the surface would be removed after association with nitrogen atoms as CN radicals [34], which is a more likely explanation given that the Ar postdischarge does not produce a significant effect on the surface (Figure 6a). Furthermore, this mechanism is in good agreement with the results observed for aluminum samples treated with similar procedures (Figure 7), where

X-ray photoelectron spectrometry (XPS) showed an increase in the amount of highly oxidized forms of nitrogen at the surface after the treatment with Ar-N_2 postdischarges as well as the appearance of hydroxide groups [14].

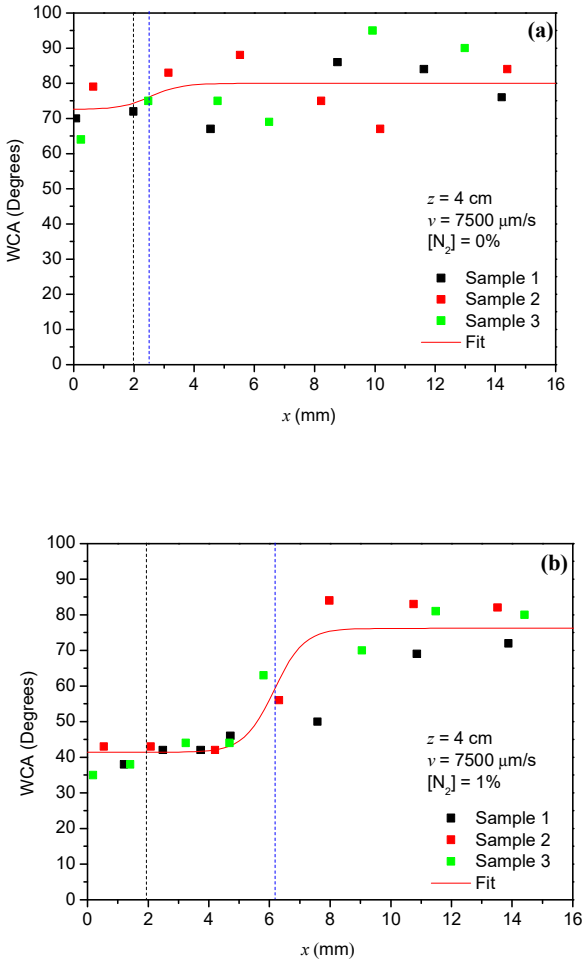

Figure 6. Water contact angle profiles after (**a**) Ar and (**b**) Ar-N_2 postdischarge treatment.

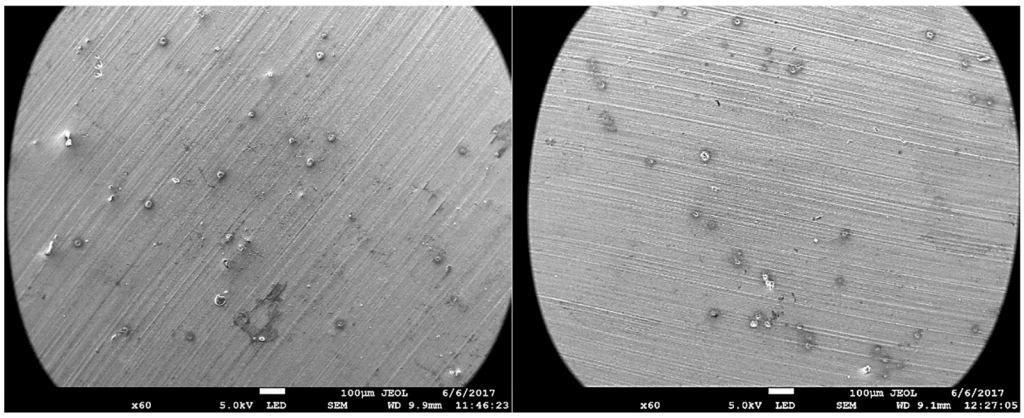

Figure 7. Scanning electron microscope image of aluminum samples before (**left**) and after (**right**) the treatment with an Ar-N_2 (1% N_2) postdischarge.

Moreover, in Figure 6b, the radius of the treated area has also been marked by a vertical blue dashed line, together with the inner radius of the tube containing the discharge, whose size appears

represented as a vertical dashed black line for comparison purposes. For the considered conditions, the radius of the treated zone is of 6.1 ± 0.4 mm, which is three times the inner radius of the tube containing the discharge, thus meaning that the postdischarge expands before reaching the sample, and might be able to interact with the surrounding atmosphere.

The influence of varying the treatment distance, z, for the same speed and nitrogen concentration can be observed comparing Figures 8 and 6b. For increasing treatment distances from 2 to 6 cm, WCA_{min} rising from values of 25° to 65°, respectively, revealing a decrease in the cleaning effect of the postdischarge as its length increases. This fact agrees with the proposed mechanism of action mainly due to the active species of postdischarge. When the distance from the end of the discharge increases, the amount nitrogen excited species decreases and, consequently, the capability of the postdischarge to modify the hydrophobicity of the material surface. These results are in agreement with those reported for similar treatments [14].

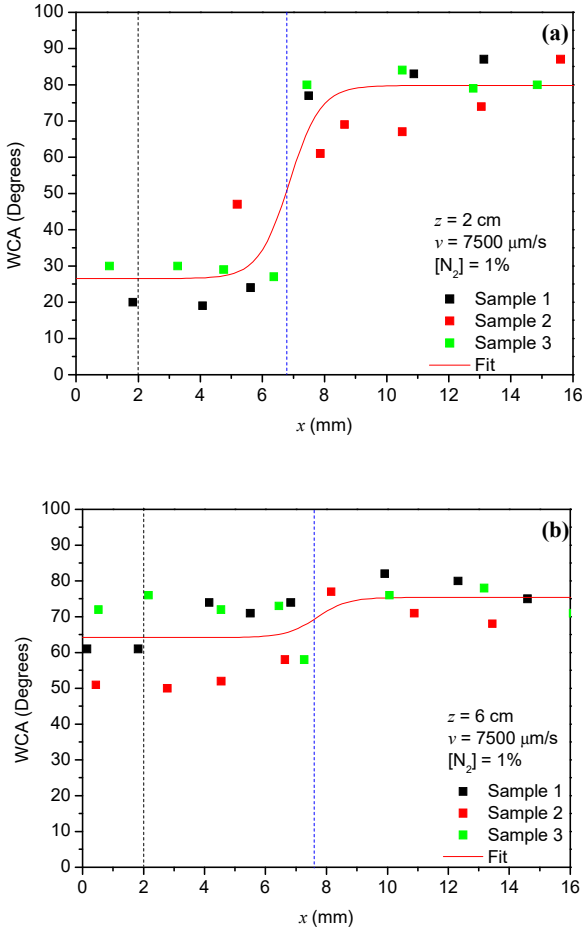

Figure 8. Water contact angle profile after Ar-N_2 postdischarge treatment at different distances measured from the end of the discharge: (**a**) $z = 2$ cm and (**b**) $z = 6$ cm.

The width of the treatment profile is not significantly influenced by the distance of the treatment, showing a radii of 6.9 ± 0.3 and 7.7 ± 1.3 mm for distances of 2 and 6 cm, respectively. This indicates that, for the considered conditions, the postdischarge expands once the gas exits the tube containing the discharge within a relatively short distance (≤2 cm). From this point, the transversal section maintains practically a radius value around 6–7 mm. This happens because the outer layers of the gas shield the inner part of the postdischarge and reduce the interaction between the postdischarge and the surrounding atmosphere. A similar behavior has been described for plasma gas used to generate a microwave plasma torch [31].

The effect of treating the samples at different treatment speeds; i.e., at different treatment times, while keeping the distance at 4 cm is shown in Figure 9. Comparing with the results obtained in Figure 6b, reducing the speed of the treatment to 5000 μm/s does not significantly affect the effect of the treatment, resulting in WCA_{min} values of 45°, and a radius of the treatment spot of 5.8 ± 0.3 mm, similar to those obtained for a treatment speed of 7500 μm/s. Further reduction of the treatment speed to 500 μm/s leads to a radius of the treatment spot of 4.4 ± 1.1 mm, which reasonably agrees with the previous ones. The most significant difference in the case when the sample is treated for a longer time, i.e., lower treatment velocity, is that WCA_{max} decreases to values around 60°. It might be likely a result of heating of the area adjacent to the treatment spot and the subsequent vaporization of hydrocarbons present at the surface. Even though the effect of heating was discarded in previous studies for speeds of 7500 μm/s [14], it may still play a role for lower speeds. In any case, it must be taken into account that, for this case, dispersion in the WCA results is larger than in the previous ones.

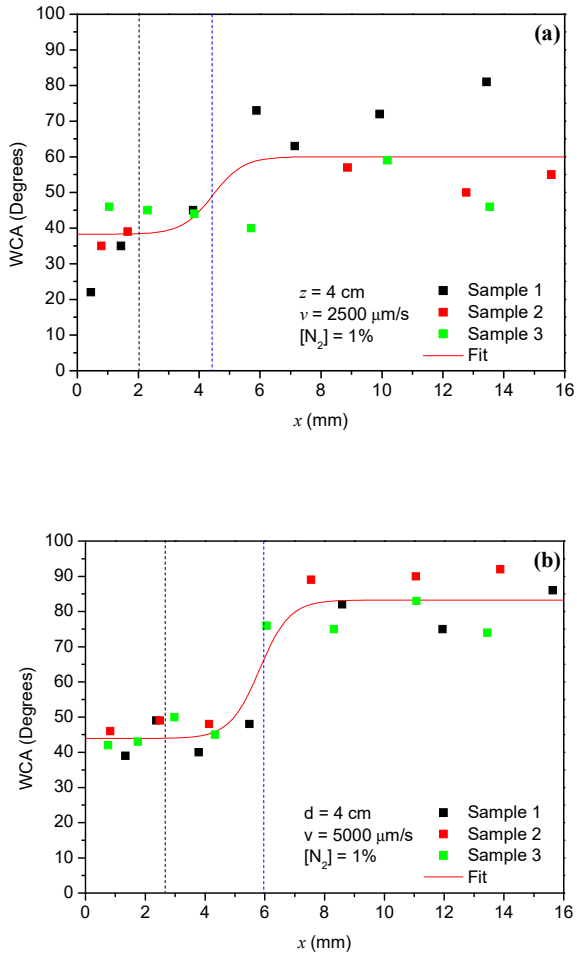

Figure 9. Water contact angle profile after Ar-N_2 postdischarge treatment at different speeds: (**a**) 2500 μm/s and (**b**) 5000 μm/s.

4. Conclusions

The parameters influencing the spatial distribution of the treatment of an aluminum surface by an atmospheric pressure remote plasma have been investigated using the sessile drop method. The position of the sample in the postdischarge (z) has been found to have a large impact in the wettability property of the treated sample, with lower WCA for positions closer to the end of the discharge. On the other hand, the treatment speed (v) has been shown to have a little impact on the spatial distribution of the treatment, except for the lowest velocity, where a lowering in the WCA values of the outer zone of the profile has been found, probably due to heating of the adjacent zones.

Neither the distance to the plasma end (z) nor the treatment speed (v) have a significant impact on the radius of the spot, which remains approximately constant (6–7 mm) regardless of the considered conditions ($2 < z < 6$ cm, $2500 < v < 7500$ μm/s).

The possible cleaning and activation mechanism was discussed to the light of the spectra emitted by the postdischarge, where active species with long lifetimes are draught from the discharge by the action of the gas flow. The limited effect of pure argon postdischarges on the surface for the treating conditions considered suggests that active species of nitrogen are the main agent responsible for the action of the postdischarge on the aluminum surfaces. Due to the absence of significant OH emissions at relatively short distances, the direct implantation of these radicals might be discarded, suggesting that interaction with other active and/or energetic species in the discharge is responsible for the increase of the surface wettability of the treated samples.

Author Contributions: J.M. designed and performed the experiments, M.D.C. analyzed data, J.M., R.R. and M.D.C. wrote and reviewed the paper.

Funding: This research was funded by Universidad de Cordoba (Spain), grant number MOD 4.1 PP2017-2018 (XXII-XXIII Programa Propio de Fomento de la Investigación).

Acknowledgments: This work was supported by XXII-XXIII Programa Propio de Fomento de la Investigación de la Universidad de Córdoba (Spain) (MOD 4.1 PP2017-2018).

Conflicts of Interest: The authors declare no conflict of interest.

References

1. Richard Prabakar, S.J.; Hwang, Y.-H.; Bae, E.G.; Lee, D.K.; Pyo, M. Graphene oxide as a corrosion inhibitor for the aluminum current collector in lithium ion batteries. *Carbon* **2013**, *52*, 128–136. [CrossRef]
2. Liu, Y.; Zhang, J.; Li, S.; Wang, Y.; Hana, Z.; Rena, L. Fabrication of a superhydrophobic graphene surface with excellent mechanical abrasion and corrosion resistance on an aluminum alloy substrate. *RSC Adv.* **2014**, *4*, 45389. [CrossRef]
3. Polini, W.; Sorrentino, L. Improving the wettability of 2024 aluminum alloy by means of cold plasma treatment. *Appl. Surf. Sci.* **2003**, *214*, 1–4. [CrossRef]
4. Morent, R.; de Geyter, N.; Verschuren, J.; de Clerck, K.; Kiekens, P.; Leis, C. Non-thermal plasma treatment of textiles. *Surf. Coat. Technol.* **2008**, *202*, 3427–3449. [CrossRef]
5. Xu, X. Dielectric barrier-discharge-properties and applications. *Thin Solid Films* **2001**, *390*, 237–242. [CrossRef]
6. Prysiazhnyi, V.; Matoušek, J.; Černák, M. Steel surface treatment and following aging effect after coplanar barrier discharge plasma in air, nitrogen and oxygen. *Chem. Listy* **2012**, *106*, 1475–1481.
7. Prysiazhnyi, V. Atmospheric pressure plasma treatment and following aging effect of chromium surfaces. *J. Surf. Eng. Mater. Adv. Technol.* **2013**, *3*, 138–145. [CrossRef]
8. Bónová, I.; Zahoranová, A.; Kováčik, D.; Zahoran, M.; Mičušík, M.; Černák, M. Atmospheric pressure plasma treatment of flat aluminum surface. *App. Surf. Sci.* **2015**, *331*, 79–86. [CrossRef]
9. Prysiazhnyi, V.; Zaporojchenko, V.; Kersten, H.; Černák, M. Influence of humidity on atmospheric pressure air plasma treatment of aluminum surface. *Appl. Surf. Sci.* **2012**, *258*, 5467–5471. [CrossRef]
10. Prysiazhnyi, V.; Vasina, P.; Panyala, N.R.; Havel, J.; Černák, M. Air DCSBD plasma treatment of Al surface at atmospheric pressure. *Surf. Coat. Technol.* **2012**, *206*, 3011–3016. [CrossRef]
11. Yamamoto, T.; Yoshizaki, A.; Kuroki, T.; Okubo, M. Aluminum surface treatment using three different plasma-assisted dry chemical processes. *IEEE Trans. Ind. Appl.* **2004**, *40*, 1220–1225. [CrossRef]
12. Hnilica, J.; Kudrle, V.; Potočnaková, L. Surface treatment by atmospheric-pressure surfatron jet. *IEEE Trans. Plasma Sci.* **2012**, *40*, 2925–2930. [CrossRef]
13. Shin, D.H.; Bang, C.U.; Kim, J.H.; Hong, Y.C.; Uhm, H.S.; Park, D.K.; Him, J.K. Treatment of metal surface by atmospheric microwave plasma jet. *IEEE Trans. Plasma Sci.* **2006**, *34*, 1241–1246. [CrossRef]
14. Muñoz, J.; Bravo, J.A.; Calzada, M.D. Aluminum metal surface cleaning and activation by atmospheric-pressure remote plasma. *Appl. Surf. Sci.* **2017**, *407*, 72. [CrossRef]
15. Moisan, M.; Zakrzewski, Z.; Pantel, R. The theory and characteristics of an efficient surface wave launcher (surfatron) producing long plasma columns. *J. Phy. D: Appl. Phys.* **1979**, *12*, 219–237. [CrossRef]

16. Kabouzi, Y.; Calzada, M.D.; Moisan, M.; Tran, K.C.; Trassy, C. Radial contraction of microwave sustained plasma columns at atmospheric pressure. *J. Appl. Phys.* **2002**, *91*, 1008–1019. [CrossRef]
17. Bravo, J.A.; Muñoz, J.; Sáez, M.; Calzada, M.D. Atmospheric pressure Ar-N_2 surface-wave discharge morphology. *IEEE Trans. Plasma Sci.* **2011**, *39*, 2114–2115. [CrossRef]
18. Callede, G.; Deschamps, J.; Godert, J.L.; Ricard, A. Active nitrogen atom in an atmospheric pressure flowing Ar-N_2 microwave discharge. *J. Phys. D: Appl. Phys.* **1991**, *24*, 909–914. [CrossRef]
19. Ricard, A.; Tétreault, J.; Hubert, J. Nitrogen atom recombination in high Ar-N_2 flowing post-discharges. *J. Phy. B: At. Mol. Opt. Phy.* **1991**, *24*, 1115–1123. [CrossRef]
20. Bravo, J.A.; Rincón, R.; Muñoz, J.; Sanchez, A.; Calzada, M.D. Spectroscopic characterization of argon-nitrogen Surface-wave discharges in dielectric tubes at atmospheric pressure. *Plasma Chem. Plasma Process.* **2015**, *35*, 993–1014. [CrossRef]
21. Rincón, R.; Yubero, C.; Calzada, M.D.; Moyano, L.; Zea, L. Plasma technology as a new food preservation technique. In *Microbial Food Safety and Preservation Techniques*; Ravishankar Rai, V., Bai, J.A., Eds.; CRC Press: Boca Raton, FL, USA, 2015.
22. Yuan, Y. Contact Angle and Wetting Properties. In *Surface Science Techniques*; Bracco, G., Holst, B., Eds.; Springer: Berlin, Germany, 2013.
23. Calzada, M.D.; Garcia, M.C.; Luque, J.M.; Santiago, I. Influence of the thermodynamic equilibrium state in the excitation of samples by a plasma at atmospheric pressure. *J. Appl. Phy.* **2002**, *92*, 2269. [CrossRef]
24. Kudela, J.; Odrobina, I.; Kando, M. High-speed camera study of the surface wave discharge propagation in xenon. *Jpn. J. Appl. Phy.* **1998**, *37*, 4169. [CrossRef]
25. Calzada, M.D.; Moisan, M.; Gamero, A.; Sola, A. Experimental investigation and characterization of the departure from local thermodynamic equilibrium along a surface-wave-sustained discharge at atmospheric pressure. *J. Appl. Phy.* **1996**, *80*, 46. [CrossRef]
26. Jonkers, J.; de Regt, J.M.; van der Mullen, J.A.M.; Vos, H.P.C.; de Groote, F.P.; Timmermans, E.A.H. On the electron temperatures and densities produced by the "torche à injection axiale". *Spectrochim. Acta Part B* **1996**, *51*, 1385. [CrossRef]
27. Muñoz, J.; Calzada, M.D. Experimental study on equilibrium deviations in atmospheric pressure argon/helium surface wave discharges. *Spectrochim. Acta Part B* **2010**, *65*, 1014–1021. [CrossRef]
28. Muñoz, J.; Rincón, R.; Melero, C.; Dimitrijević, M.S.; González, C.; Calzada, M.D. Validation of the van der Waals broadening method for the determination of gas temperature in microwave discharges sustained in argon–neon mixtures. *J. Quant. Spectrosc. Radiat. Transfer* **2018**, *206*, 135–141. [CrossRef]
29. Ricard, A. *Reactive Plasmas*; Société Française du Vide: Paris, France, 1996.
30. Henriques, J.; Tatarova, E.; Guerra, V.; Ferreira, C.M. Wave driven N_2-Ar discharge. I. Self-consistent theoretical model. *J. Appl. Phys.* **2001**, *91*, 5632–5639. [CrossRef]
31. Guerra, V.; Tatarova, E.; Dias, F.M.; Ferreira, C.M. On the self-consistent modeling of a traveling wave sustained nitrogen discharge. *J. Appl. Phys.* **2002**, *91*, 2648–2661. [CrossRef]
32. Rincón, R.; Muñoz, J.; Sáez, M.; Calzada, M.D. Spectroscopic characterization of atmospheric pressure argon plasmas sustained with the Torche à Injection Axiale sur Guide d'Ondes. *Spectrochim. Acta, Part B* **2013**, *81*, 26–35. [CrossRef]
33. Szili, E.J.; Al-Bataineh, S.A.; Bryant, P.M.; Short, R.D.; Bradley, J.W.; Steele, D.A. Controlling the spatial distribution of polymer surface treatments using atmospheric-pressure microplasma jets. *Plasma Processes Polym.* **2011**, *8*, 38–50. [CrossRef]
34. Mézerette, D.; Belmonte, T.; Hugon, R.; Henrion, G.; Czerwiec, T.; Michel, H. Study of the surface mechanisms in an Ar-N_2 post-discharge cleaning process. *Surf. Coat. Technol.* **2003**, *169–170*, 181–185. [CrossRef]